Trimodal Cell Tracking In Vivo: Combining Iron- and Fluorine-Based Magnetic Resonance Imaging with Magnetic Particle Imaging to Monitor the Delivery of Mesenchymal Stem Cells and the Ensuing Inflammation

Olivia C. Sehl[1,2], Ashley V. Makela[3], Amanda M. Hamilton[1], and Paula J. Foster[1,2]

[1]Imaging Research Laboratories, Robarts Research Institute and [2]Department of Medical Biophysics, University of Western Ontario, London, ON, Canada; and [3]The Institute for Quantitative Health Science and Engineering, Michigan State University, East Lansing, MI

Corresponding Author:
Olivia C. Sehl, BMSc
Robarts Research Institute, The University of Western Ontario,
1151 Richmond Street North, London, ON, N6A 5B7, Canada,
E-mail: osehl@uwo.ca

Key Words: Mesenchymal stem cells, magnetic resonance imaging (MRI), magnetic particle imaging (MPI), iron oxide nanoparticles, fluorine-19, inflammation

Abbreviations: Mesenchymal stem cells (MSCs), magnetic resonance imaging (MRI), superparamagnetic iron oxides (SPIO), proton (^{1}H), ultrasmall SPIO (USPIO), fluorine-19 (^{19}F), perfluorocarbon (PFC), magnetic particle imaging (MPI), signal to noise ratio (SNR), phosphate buffered saline (PBS), Perls' Prussian Blue (PPB), balanced steady state free precession (bSSFP), field of view (FOV), repetition time (TR), echo time (TE), flip angle (FA), bandwidth (BW), phase cycles (PC), number of excitations (NEX), point spread function (PSF), full width half maximum (FWHM)

ABSTRACT

The therapeutic potential of mesenchymal stem cells (MSCs) is limited, as many cells undergo apoptosis following administration. In addition, the attraction of immune cells (predominately macrophages) to the site of implantation can lead to MSC rejection. We implemented a trimodal imaging technique to monitor the fate of transplanted MSCs and infiltrating macrophages in vivo. MSCs were labeled with an iron oxide nanoparticle (ferumoxytol) and then implanted within the hind limb muscle of 10 C57Bl/6 mice. Controls received unlabeled MSCs (n = 5). A perfluorocarbon agent was administered intravenously for uptake by phagocytic macrophages in situ; 1 and 12 days later, the ferumoxytol-labeled MSCs were detected by proton (^{1}H) magnetic resonance imaging (MRI) and magnetic particle imaging (MPI). Perfluorocarbon-labeled macrophages were detected by fluorine-19 (^{19}F) MRI. ^{1}H/^{19}F MRI was acquired on a clinical scanner (3 T) using a dual-tuned surface coil and balanced steady-state free precession (bSSFP) sequence. The measured volume of signal loss and MPI signal declined over 12 days, which is consistent with the death and clearance of iron-labeled MSCs. ^{19}F signal persisted over 12 days, suggesting the continuous infiltration of perfluorocarbon-labeled macrophages. Because MPI and ^{19}F MRI signals are directly quantitative, we calculated estimates of the number of MSCs and macrophages present over time. The presence of MSCs and macrophages was validated with histology following the last imaging session. This is the first study to combine the use of iron- and fluorine-based MRI with MPI cell tracking.

INTRODUCTION

Mesenchymal stem cells (MSCs) have shown promising results as a cellular therapeutic. Many studies involving MSCs aim to restore damaged tissues, including bone, cartilage, tendon, adipose, and muscle tissue, through tissue regeneration (1, 2). Moreover, several proposed therapies rely on the pleiotropic effects that MSCs impose on their local microenvironment through the release of extracellular vesicles, cytokines, and tropic factors (3–5). MSCs have been shown to exert antimicrobial effects, promote local vascularization and cell growth, and modulate inflammation (1, 2, 6). MSC survival and engraftment in vivo is critical in determining therapeutic outcomes. Unfortunately, many MSCs undergo apoptosis in the days following administration owing to the stresses of administration and subsequent lack of nutrients (7, 8). Apoptotic stem cells release cytokines that attract immune cells (predominately macrophages) to the implant site. A high influx of these cells can ultimately trigger stem-cell rejection (8). The potential of MSC therapy is limited by MSC death and immune rejection; therefore, the development of a technique to

ISSN 2379-1381 https://doi.org/10.18383/j.tom.2019.00020

quantitatively monitor MSC engraftment and ensuing inflammation over time would be invaluable for evaluating the course of therapy.

Many experimental studies of MSC engraftment have been conducted using histology, which provides detailed molecular and morphological information but is limited to the interrogation of a single time point and portion of tissue. Alternatively, cellular magnetic resonance imaging (MRI) has proven to be an effective technique for noninvasive and longitudinal cell tracking (8–10). To date, most cellular MRI involves tracking cells, which are labeled with superparamagnetic iron oxide (SPIO) nanoparticles. In proton (^{1}H) MRI images, SPIO-labeled cells appear as regions of signal void. In a uniform magnetic field, SPIOs alter the net local magnetization that nearby ^{1}H atoms experience and this leads to increased R2* relaxation rates of these ^{1}H atoms. These voids occupy a volume that is greater than the labeled cells, an effect referred to as the blooming artifact. This effect can lead to enhanced sensitivity of cell detection (11), but it poses challenges for accurate quantification of cell number. Measuring the volume of signal voids is one metric to estimate the number of cells present; however, this is not a direct relationship. One other limitation of SPIO-based cell tracking is lack of specificity in some tissues (9, 12). There is some ambiguity when identifying these cells in vivo, as other regions in anatomic MRI appear dark (ie, the air-filled lungs).

Ultrasmall superparamagnetic iron oxides (USPIOs) are a subset of iron oxides used for MRI cell tracking. These nanoparticles are ~30 nm in diameter and are coated in dextran, and thus, they are biocompatible and biodegradable. Ferumoxytol is one such USPIO that is FDA-approved for iron replacement therapy for the treatment of anemia in patients and may be used off-label for iron-based MRI cell tracking (13, 14). In this study we will use ferumoxytol for iron oxide cell labeling of MSC, as it is the most clinically applicable agent.

Fluorine-19 (^{19}F) MRI cell tracking is an alternative to iron oxide-based MRI. In this technique, cells are labeled with perfluorocarbon (PFC) nanoemulsions and detected with ^{19}F MRI in a hotspot image. Since there is little endogenous ^{19}F within biological tissues, these cells can be visualized with high specificity. The signal intensity of these images is directly linear to the number of ^{19}F atoms, which allows for the quantification of ^{19}F labeled cells in vivo (8, 9, 15). One limitation of ^{19}F-based cell tracking is that the sensitivity of detection is much less than iron oxide agents, requiring a minimum of 10^{3} - 10^{5}-labeled cells per imaging voxel. PFC agents are clinically approved for cell tracking (16).

Magnetic particle imaging (MPI) is an emerging modality that directly detects SPIO nanoparticles. Similar to ^{19}F MRI, MPI produces positive contrast images of the distribution of labeled cells. MPI signal is linearly related to the quantity of iron oxide tracer that allows for accurate quantification of SPIO-labeled cells (13, 17). It is not feasible to achieve this reliable specificity and quantification in SPIO-based MRI cell tracking, although SPIO-based MRI cell tracking may have superior detection sensitivity depending on tissue contrast. MPI has the potential to overcome the limitations of ^{19}F MRI (sensitivity) and iron-based MRI (specificity and quantification).

In this study, we use ferumoxytol for labeling and detecting MSCs with MPI, which has recently been shown to permit quantification of MSCs transplanted in a mouse model of osteoarthritis (13). This group also showed that MPI of ferumoxytol-labeled cells was sensitive to changes in cell number in vivo over time, whereas the voids detected in ^{1}H MRI did not detect this change.

One strategy for detecting immune cells in vivo involves the intravenous administration of the labeling agent. This leads to uptake of the agent by phagocytic cells of the reticuloendothelial system (predominately macrophages) in vivo (8, 10, 18). MRI is typically performed 1 day after the administration of the cell labeling agent to permit for the clearance of intravascular agent and the accumulation of the label into cells.

Our aim is to combine the use of iron-based MRI, ^{19}F MRI, and MPI cellular imaging technologies to monitor and quantify the persistence of transplanted MSCs and infiltrating macrophages in vivo. These 3 modalities are complementary and provide additional information (specificity, sensitivity, and quantification of cell number) when integrated together. We explored the ability to label, detect, and quantify MSCs with ferumoxytol for detection in ^{1}H MRI and MPI images, and infiltrating macrophages with PFC for ^{19}F MRI detection.

METHODOLOGY

MSC Preparation

MSCs derived from the bone marrow of C57BL/6 mice (MUBMX-01101 [BE], Cedarlane, Burlington, Ontario, Canada) were cultured at 37°C and 5% CO_2 in low-glucose Dulbecco's modified Eagle's medium (Thermo Fisher Scientific, Waltham, Massachusetts). MSCs were passaged every 2 - 3 days for 10 days. When 80%– 90% confluence was met, these cells were labeled with 50.4 μg Fe/mL ferumoxytol (Feraheme, AMAG Pharmaceuticals), along with 60 μg/mL protamine sulfate and 3 U/mL heparin (Sandoz Canada), as per protocol by Thu et al. (19). After overnight incubation, the cells were washed 3 times with phosphate-buffered saline (PBS) before and after trypsin dissociation. Cell counting and viability was determined using the trypan blue exclusion assay (using Countess Automated Cell Counter; Invitrogen). Further, 2×10^{5} ferumoxytol and unlabeled cells were collected for Perls' Prussian Blue (PPB) staining to assess iron labeling (20). Cell pellets (1×10^{6} MSCs) were collected to determine iron content using MPI (see below).

Animal Model

15 C57B1/6 mice (Charles River, Canada, Pittsburgh) were obtained and cared for in accordance with the standards of the Canadian Council on Animal Care, under an approved protocol by the Animal Use Subcommittee of Western University's Council on Animal Care. 1×10^{6} UPSIO-labeled MSCs in 25-μL PBS were implanted to the hind limb muscle of 10 immune-competent C57B1/6 mice (day 0). A second cohort of control mice (n = 5) received 1×10^{6} unlabeled MSCS in 25-μL PBS. Immediately after MSC implantation, mice were administered 200-μL PFC agent (V-Sense, CelSense Inc.) intravenously via the tail vein to label phagocytic immune cells in situ. Injections were performed under 2% isoflurane in 100% oxygen anesthesia.

^{1}H/^{19}F MRI Acquisition

One and 12 days following MSC implantation, in vivo MRI images of all mice (n = 15) were acquired on a 3 T clinical scanner

(Discovery MR750, General Electric) using a 4.31- × 4.31-cm-diameter $^{1}H/^{19}F$ dual-tuned RF surface coil (Clinical MR Solutions, Wisconsin) as previously described (21). Both ^{1}H and ^{19}F images were acquired with 3-dimensional (3D) balanced steady-state free precession (bSSFP) sequences. Mice were anesthetized with 2% isoflurane in 100% oxygen during these scans.

^{1}H imaging parameters were as follows: field of view (FOV) = 60 × 30 mm; matrix size = 150 × 75, slice thickness = 0.4 mm (0.4 × 0.4 × 0.4 mm^3 resolution), repetition time (TR)/echo time (TE) = 12.8 / 6.4 milliseconds, flip angle (FA) = 20°, bandwidth (BW) = ±31.25 kHz, phase cycles (PC) = 12, number of excitations (NEX) = 1, total scan time = 9 minutes. ^{19}F imaging parameters were: FOV = 60 × 30 mm, matrix = 60 × 30, slice thickness = 1 mm (1 × 1 × 1 mm^3 resolution), TR/TE = 5.6 / 2.8 milliseconds, FA=72°, BW = ±10 kHz, PC = 1, NEX = 100, total scan time = 18 minutes.

Quantification of Signal Loss Due to Iron-Labeled MSC

^{1}H images were assessed for abnormal regions of signal loss (dark regions), in the area where MSCs were implanted. These regions were manually contoured over multiple ^{1}H slices to measure the signal void volume (Osirix, Pixemo SARL, Bernex, Switzerland).

^{19}F Signal Quantification

^{19}F images were overlaid onto ^{1}H images (Osirix, Pixemo SARL) for anatomical reference. ^{19}F signal in the limb ipsilateral to the MSC implant was manually delineated and quantified relative to reference tubes of known ^{19}F content (3.33×10^{16} $^{19}F/\mu L$). Owing to the presence of phagocytic immune cells in the bone marrow (BM) and lymph nodes (LN), any ^{19}F signal in the contralateral limb was subtracted from the ipsilateral limb, to isolate the ^{19}F signal detected in the region of MSC implantation.

Evaluation of Ferumoxytol as an MPI Tracer

The particle relaxometer module (RELAX™) on the MOMENTUM™ system (Magnetic Insight Inc., Alameda, California) was used to characterize ferumoxytol as an MPI tracer. In this mode, the localizer gradient field is switched off and a negative magnetic field is turned on and then switched to a positive field (and vice versa). As a result, iron nanoparticles are driven from a negative magnetic saturation to positive (positive scan) and vice versa (negative scan). This measures the point spread function (PSF) of the nanoparticles and allows for measurements of properties such as full-width half-maximum (FWHM) (spatial resolution) and signal per gram of iron (sensitivity) (22, 23). We used FWHM to define tracer resolution, according to the Houston criterion (24). The shift between the positive and negative PSF is a result of magnetic relaxation as described in some studies (23, 25). We acquired PSFs for 30 μg and 5.5 μg (in 1 μL) ferumoxytol.

MPI Acquisitions

For 5 of the 10 mice that had ferumoxytol-labeled MSC implanted and that were imaged with MRI, full-body in vivo MPI images of mice were acquired. Image acquisition occurred on days 1, 5, and 12 following MSC implantation, on a MOMENTUM™ system (Magnetic Insight Inc.) using the 3D isotropic mode. In this mode, tomographic images were acquired using a 5.7 T/m gradient, 35 projections, 1 average, in an FOV of 12 × 6 × 6 cm, for a total scan time of ~1 h per mouse. We have included day 5 images as an explorative, intermediate time point, to assess MPI detection of MSCs over time. Mice were anesthetized with 2% isoflurane in 100% oxygen during these scans. 3D isotropic images of MSC pellets were acquired using the same parameters on day 0.

MPI Calibration and Signal Quantification

Calibration lines were produced to determine the relationship between iron content in ferumoxytol (30 mg/mL) and MPI signal. To construct this line, 1 μL samples of ferumoxytol were scanned in the same mode as in vivo images (3D isotropic). Samples of iron content over 2 orders of magnitude were tested: 0.75 μg, 1.125 μg, 1.5 μg, 2.25 μg, 3 μg, 7.5 μg, 11.25 μg, 15 μg, 22.5 μg, and 30 μg iron.

All MPI images were displayed in full dynamic range and assessed for MPI signal corresponding to the samples (calibration samples, MSC pellets, or MSCs in vivo) with spatial reference to fiducial markers (Osirix, Pixemo SARL). To quantify the MPI signal in a specific region of interest (ROI), a 3D semi-automatic segmentation tool was used. Before delineating these ROIs, the window/level (W/L) was adjusted to each specific region, such that the full dynamic range of this region was displayed. Total MPI signal for the delineated volume was calculated by multiplying mean signal by volume. With samples of increasing iron content, both MPI signal and volume of the ROI increase. Total MPI signal was plotted against iron content to derive calibration lines, and this relationship was used to quantify iron content in MSC pellets and MSCs in vivo. All MPI images, including the calibration, MSC pellets, and in vivo images, were delineated and analyzed in the same way to ensure consistency.

Histological Analysis

Following the last imaging sessions on day 12, mice were euthanized by isoflurane overdose and then perfusion-fixed with 4% paraformaldehyde. The right limb muscle of mice was excised and paraffin-embedded. Embedded tissues were sectioned (5 μm in thickness) every 400 μm to ensure entire sampling of the tissue. These sections were stained with hematoxylin and eosin for general tissue morphology, PPB and nuclear fast red counterstain to identify the presence of ferumoxytol, or F4/80 immunohistochemical staining to identify macrophages. For F4/80 staining, sections underwent antigen retrieval in sodium citrate buffer, permeabilized using 0.4% Triton X-100 (Sigma-Aldrich, Oakville, Ontario, Canada), followed by overnight incubation in rat antimouse F4/80 primary antibody [1:100 dilution] (ab16911, Abcam). The next day, sections were incubated with biotinylated goat antirat IgG antibody [1:300 dilution] (BA-9401, Vector Laboratories) and then processed with ABC solution (PK4000, Vector Laboratories, Burlington, Ontario, Canada). Lastly, the slides were incubated in 3,3′-diaminobenzidine tetrahydrochloride (DAB) substrate solution (SK-4100, Vector Laboratories) and counterstained with hematoxylin. Histological images were acquired on the EVOS Imaging System (M7000, Thermo Fischer Scientific).

Statistical Analysis

Linear correlations were conducted between total MPI signal and iron content to determine Pearson's correlation coefficient. Student *t*-tests were used to evaluate temporal changes in signal

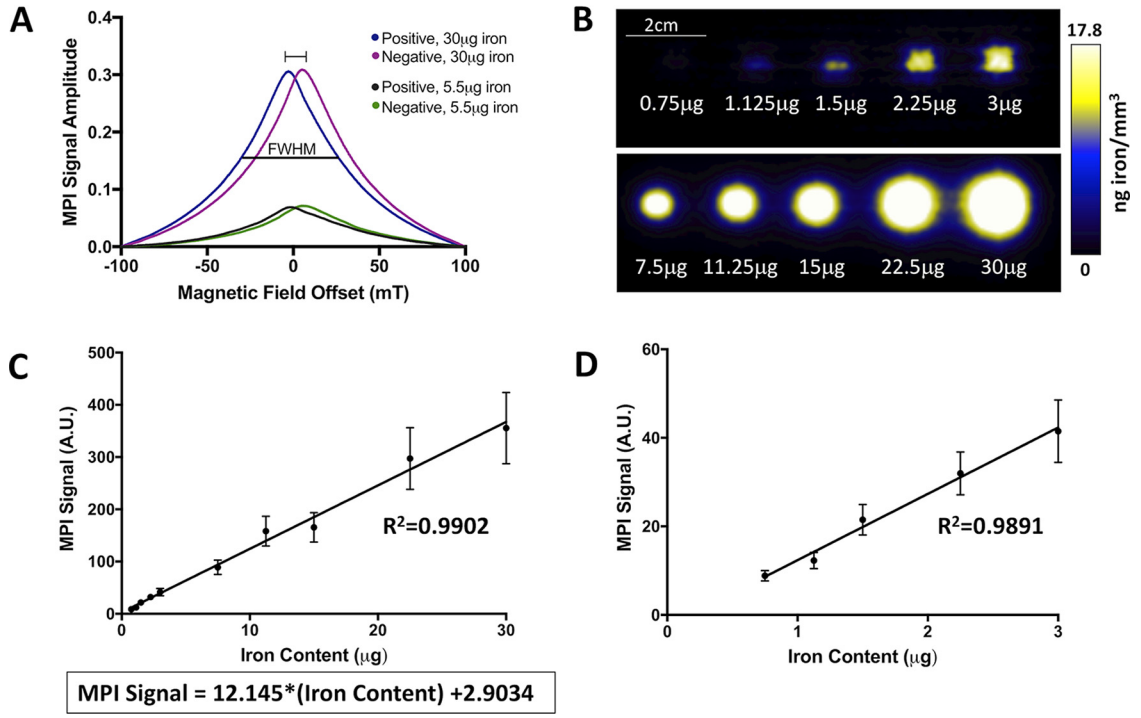

Figure 1. Ferumoxytol evaluation and magnetic particle imaging (MPI) signal calibration. Relaxometer data showing the point spread functions for 30 μg and 5.5 μg ferumoxytol (A). The full-width half-max (FWHM) is labeled for the positive 30-μg iron relaxometer data. A projection of 3-dimensional MPI images (in 3D isotropic mode) of ferumoxytol samples (B) used to create a calibration line (C). The relationship between iron content and MPI signal remains linear at low concentrations of iron (D).

void volumes and ^{19}F signal (day 1 vs 12). One-way ANOVA was used to determine statistical changes in MPI signal over time (days 1, 5, and 12). These analyses were conducted using Prism software (8.0.2, GraphPad Inc.), where $P < .05$ was considered statistically significant. Values are presented as mean ± standard deviation.

RESULTS

Evaluation of Ferumoxytol as an MPI Tracer

We used the relaxometer mode on the Momentum™ scanner to measure the FWHM of 30 μg and 5.5 μg (in 1 μL PBS) ferumoxytol. As seen in Figure 1A, we measured a FWHM of 66.335 mT. For a 6.1 T/m gradient, the resolution of this ferumoxytol is 1.088 cm. The amplitude of the 30 μg PSF was ~4.5 times the height of the 5.5-μg PSF.

Relationship Between Iron Content and MPI Signal

We acquired images of ferumoxytol samples with known iron content (Figure 1B). These samples were separated by 2 cm on the MPI bed (5 samples/scan). There was a strong linear relationship (R^2 = 0.992, $P < .001$) between iron content and MPI signal (arbitrary units, A.U.) (Figure 1C). This relationship holds for small quantities of iron that are relevant for our investigation (Figure 1D). The equation of the line is: MPI Signal = 12.145 × (Iron content) + 2.9034. Using this relationship, iron content may be determined for a given MPI signal. We used these calibration lines to quantify iron content in ferumoxytol-labeled MSC pellets and ferumoxytol-labeled MSCs in vivo.

Assessment of MSC Labeling with Ferumoxytol

Uptake of ferumoxytol by MSCs was assessed using PPB staining (Figure 2, A and B), and iron content in 1×10^6, 0.5×10^6, and 0.25×10^6 cells was quantified using MPI (Figure 2C). These 2 techniques indicated that MSCs were adequately labeled, with 2.430 ± 0.211 pg iron/cell.

We also showed that there is a relationship between MPI signal and the number of ferumoxytol-labeled MSCS in the pellet on day 0. For pellets containing 0.25×10^6, 0.5×10^6, and 1×10^6 cells, iron content was determined to be 0.876 μg, 1.227 μg, and 2.208 μg, respectively (Figure 2D). The viability of these cells did not change with MSC labeling (97% viability before and after labeling).

Detection of Ferumoxytol-Labeled MSCS with ^{1}H MRI and MPI and PFC-Labeled Immune Cells with ^{19}F MRI

Figure 3 shows ^{1}H, ^{19}F, and MPI images of mice which received 1×10^6 ferumoxytol-labeled MSCs (A-C) or unlabeled-MSCs (D,E). In ^{1}H MRI, ferumoxytol-positive MSCs were detected as regions of signal void at the site of implantation in all mice (n = 10), 1 and 12 days following MSC implantation (Figure 3A, labeled Fe). These voids were easily distinguishable on day 1 but were more challenging to locate by day 12 owing to the size

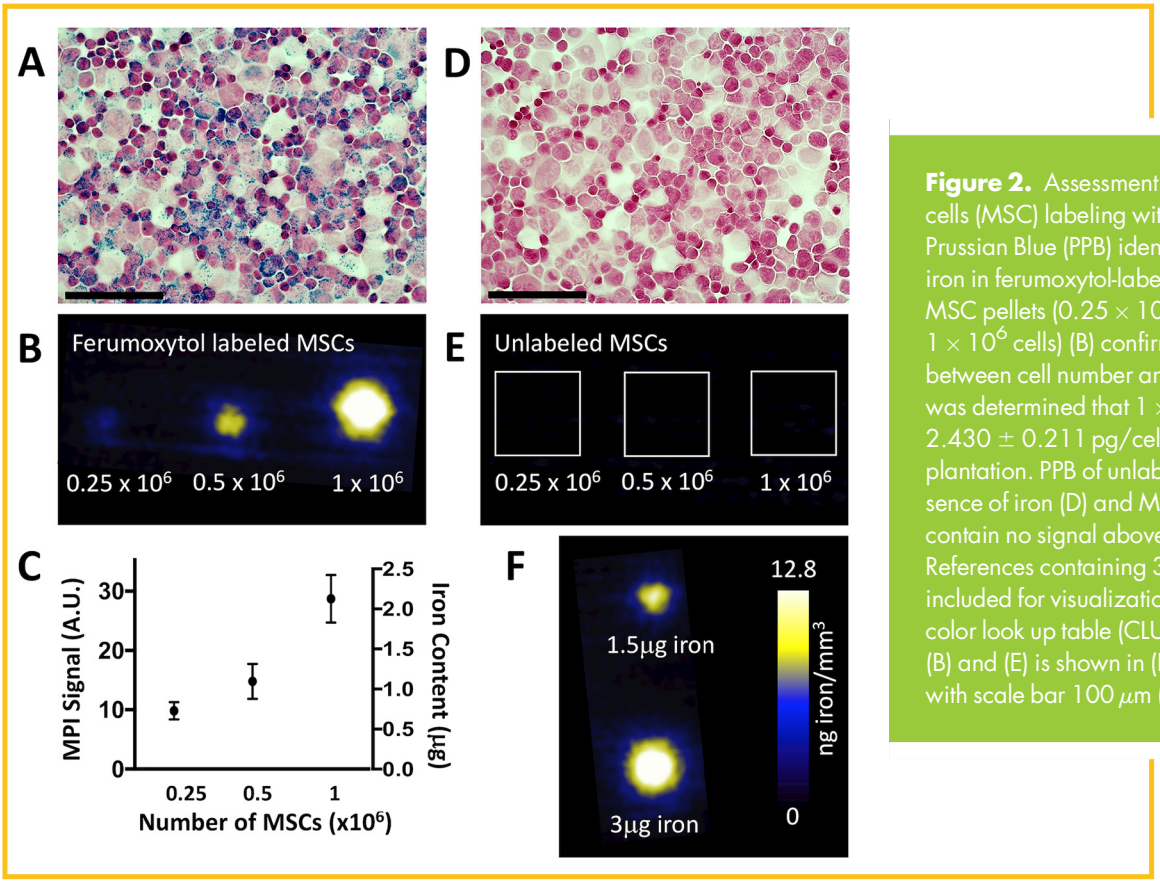

Figure 2. Assessment of mesenchymal stem cells (MSC) labeling with ferumoxytol. Perls' Prussian Blue (PPB) identifies the presence of iron in ferumoxytol-labeled MSCs (A). (B) MPI of MSC pellets (0.25×10^6, 0.5×10^6, and 1×10^6 cells) (B) confirms the linear relationship between cell number and MPI signal (C). It was determined that 1×10^6 cells contained 2.430 ± 0.211 pg/cell on the day of MSC implantation. PPB of unlabeled cells reveals the absence of iron (D) and MPI images of cell pellets contain no signal above background levels (E). References containing 3 μg and 1.5 μg were included for visualization of the signal (F). The color look up table (CLUT) for the MPI images in (B) and (E) is shown in (F). 40× magnification with scale bar 100 μm (A, D).

reduction of the voids. In some cases, these voids were difficult to distinguish based on other anatomical features that appear dark on ^{1}H MRI.

^{19}F MRI was overlaid to ^{1}H images and it revealed PFC uptake in the bone marrow (BM) and lymph nodes (LN), as well as in the muscle surrounding the MSC implant (Figure 3B). This is due to the presence of phagocytic immune cells in these regions. ^{19}F images were first displayed according to their full dynamic range, then W/L to eliminate the background noise in the final images. This signal is unambiguous and directly related to the number of ^{19}F atoms present in the tissue, which allows for assessment of relative cell number.

Ferumoxytol-labeled MSCs were also detected with MPI 1, 5, and 12 days after MSC implantation (Figure 3C; and see online Supplementary Figure 1). These MPI images were windowed to display the full dynamic range from a 1.5-μg ferumoxytol reference (not shown). In day 12 images, MPI signal generated from ferumoxytol-positive MSCs was diminished but more clearly visible with windowing. In MPI images, signal was also detected in the gut regions, presumably owing to the presence of iron in mouse feed. Mouse feed was imaged separately by MPI and had substantial iron content (shown in online Supplementary Figure 2).

In control mice that received unlabeled MSCs (n = 5), no regions of signal voids were detected in ^{1}H images (Figure 3D). In these same mice, ^{19}F signal was detected in the LNs, BM, and in the muscle where the MSC implant occurred, similar to the mice which received ferumoxytol-labeled MSCs (Figure 3E).

Quantification of Temporal Changes in Iron Voids, ^{19}F Signal, and MPI Signal

Over 12 days, the measured iron void volumes in ^{1}H images declined in all 10 mice, by 62% on average ($P = .0003$) (Figure 4A). On day 1, the average void was 9.216 ± 4.136 mm^3 and by day 12, 3.523 ± 2.217 mm^3.

^{19}F signal, detected from PFC-labeled immune cells, was detected in both limbs in all 15 mice on day 1 and 12 (Figure 4B). On day 1, ^{19}F signal in the limb ipsilateral to the MSC implant was $(1.866 \pm 0.5825) \times 10^{19}$ spins and $(2.522 \pm 2.101) \times 10^{18}$ spins in the contralateral limb. Signal in the contralateral limb was only present in the bone marrow and LNs. The difference in ^{19}F signal between these limbs, representing signal solely from immune infiltration as a result of the MSC implantation, was $(1.614 \pm 0.6604) \times 10^{19}$ ^{19}F spins. On day 12, $(1.560 \pm 0.6535) \times 10^{19}$ ^{19}F spins were present in the ipsilateral limb and $(8.518 \pm 7.227) \times 10^{18}$ spins in the contralateral limb, resulting in a difference of $(1.470 \pm 0.6565) \times 10^{19}$ ^{19}F spins. There was no significant difference ($P = .148$) in the ^{19}F signal resulting from MSC implantation (ie, the differences between limbs) when comparing signal on day 1 and day 12. This indicates the persistent infiltration of immune cells. There was no significant difference ($P = .841$) in ^{19}F signal between mice administered ferumoxytol-labeled MSCs ($1.530 \pm 0.746 \times 10^{19}$, n = 10) and unlabeled MSCs ($1.577 \pm 0.487 \times 10^{19}$, n = 5).

In vivo iron content in MSCs measured by MPI on day 1 (1.510 ± 0.206 μg, n = 5 mice) was significantly different from day 12 (0.492 ± 0.131 μg, n = 5 mice; $P = .002$) (Figure 4C). We

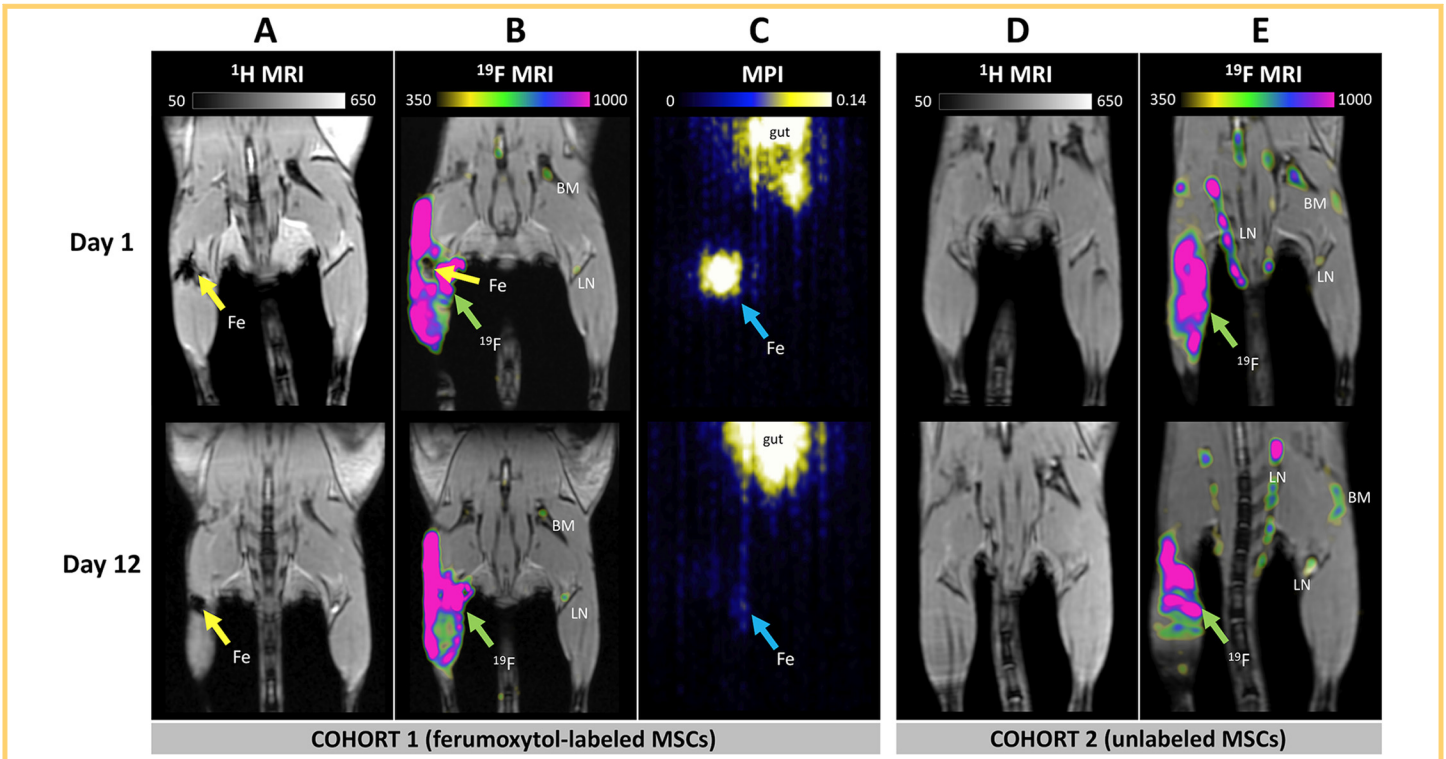

Figure 3. In vivo ^{1}H/^{19}F MRI and MPI. In ^{1}H images, ferumoxytol-positive MSCs were detected as regions of signal loss 1 and 12 days following MSC implantation (labeled Fe) (A). In ^{19}F MRI, PFC-positive immune cells are detected in the bone marrow (BM), lymph nodes (LN), and in the muscle surrounding the MSC implant (B). Ferumoxytol-positive MSCs are also detected in MPI images as bright spots (labeled Fe) (C). In these images, iron in the gut of the mice (ie, food) is also detected by MPI. The range of the MPI images is 0–0.14 arbitrary units, which is equivalent to 0–9.8 ng iron/mm^{3}. Mice that received unlabeled MSCs (controls) had no signal voids present in ^{1}H MRI (D) and ^{19}F signal persisting (E), in response to the implant. The CLUT is displayed above each image. All images of the same type are windowed identically for comparison.

imaged 3 of these mice on day 5 and the measured iron content ($1.072 \pm 0.154\,\mu g$) was also significantly higher than iron content measured on day 12 ($P = .014$). Under the assumption that these cells retain iron in vivo (2.430 ± 0.211 pg/cell), we detected $6.21 \pm 0.847 \times 10^{5}$ MSCs 1 d after implantation (n = 5 mice), $4.410 \pm 0.634 \times 10^{5}$ MSCs on day 5 (n = 3 mice), and $2.027 \pm 0.539 \times 10^{5}$ MSCs on Day 12 (n = 5 mice) (Figure 4D).

These quantitative findings are summarized in Table 1.

Microscopy and Immunohistochemistry

MSCs were identified in hematoxylin and eosin sections among connective and muscular tissue (Figure 5A). PPB staining verified the presence of ferumoxytol in these MSCs (Figure 5B). F4/80 staining with DAB identified macrophages infiltrating the MSCs (Figure 5C). These are directly adjacent sections.

DISCUSSION

We have detected and quantified the presence of MSCs and infiltrating macrophages over time using a unique combination of cellular imaging technologies. MSCs were labeled with ferumoxytol and detected in ^{1}H images as regions of negative signal (signal void) and in MPI images as regions of positive signal. Macrophages that accumulate at the site of MSC implantation were labeled in vivo with a PFC agent, then detected with ^{19}F MRI. The direct quantification of MPI and ^{19}F MRI signal was used to estimate the relative number of MSCs and macrophages over time. This multimodality imaging approach allowed for the confirmation of MSC delivery, the measurement of MSC number over time (post implantation), and quantification of inflammation.

Ferumoxytol as a Dual ^{1}H MRI and MPI Cell Tracking Agent

In this study, we measured a decrease in the volume of signal loss generated by ferumoxytol-labeled MSCs in ^{1}H images and a decrease in MPI signal detected over 12 days following MSC implantation. This occurred in all mice and is consistent with several previous MRI cell tracking studies from our laboratory (8, 15, 26). Microscopy obtained on day 12 confirmed that PPB-positive cells were present in muscle tissue at the site of implantation. The decrease in the region of signal loss in MR images and the MPI signal is likely because of MSC apoptosis and clearance of these cells by the immune system. The use of MRI to measure signal void volume gave us an indication that there were fewer cells at day 12 than at day 1. However, this is not a direct measure of the number of MSCs present owing to the blooming

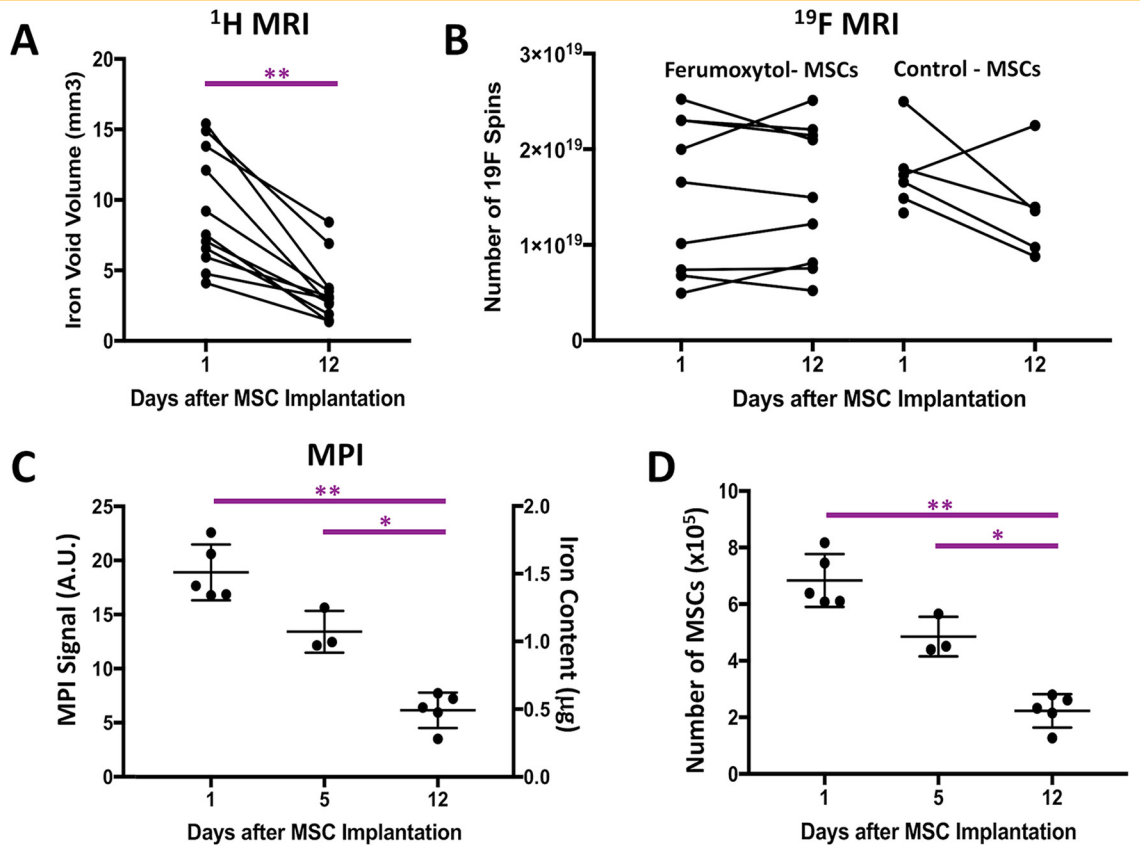

Figure 4. The volume of signal void in ^{1}H MR images created by ferumoxytol-labeled MSCs declined over 12 days (by 64%) in all 10 mice (A). ^{19}F signal detected from perfluorocarbon (PFC)-positive immune cells remained constant over these 12 days in all 15 mice (B). There was no significant difference in ^{19}F signal between mice with ferumoxytol-labeled (n = 10 mice) or unlabeled (n = 5 mice) MSCs. MPI signal and iron content (determined by MPI) declined over 12 days (67% reduction between days 1 and 12) in all 5 mice (C). The number of MSCs (estimated using MPI data) also declined over time in these same mice (D).

artifact and the nonlinear relationship between signal loss and cell number. With MPI we detected a decrease in positive signal produced by ferumoxytol-labeled MSCs over 12 days. This finding was in agreement with our MRI measurements; however, the MPI signal is directly related to iron concentration, which can be related back to MSC number. We can estimate the number of MSCs in vivo from the MPI data by comparing the measurements of MPI signal with the mean iron uptake per cell for MSC labeled in vitro. MPI data for cell samples showed 2.4 pg iron per MSC on average. This was used to estimate the number of MSCs in vivo over time (Figure 4, C and D).

The use of ferumoxytol as a tracer for both iron-based ^{1}H MRI and MPI cell tracking is appealing, as it is a clinically translatable iron nanoparticle. However, other iron nanoparticles (ie, ferucarbotran, an SPIO) have superior MPI SNR and spatial resolution compared with ferumoxytol (13). In this study we reported an FWHM of 1.088 cm for 30 μg of ferumoxytol (30 μg iron/μL). We also reported a PSF for 5.5 μg ferumoxytol (in 1 μL PBS) to

Table 1. Summary of Temporal Changes Measured in ^{1}H MRI, MPI, and ^{19}F MRI Resultant of the Presence of Ferumoxytol-Labeled MSCs and PFC-Labeled Macrophages

Measurement	Day 1	Day 12	*P*
Iron Void Volume by ^{1}H MRI (n = 10)	9.2 ± 4.1mm^3	3.5 ± 2.2 mm^3	<.001
MPI Signal (n = 5)	18.8 ± 2.9 A.U.	4.4 ± 1.9 A.U.	.002
^{19}F Signal surrounding MSCs with iron (n = 10)	1.5 ± 0.8 x10^{19}	1.5 ± 0.7 × 10^{19}	.953
^{19}F Signal in control mice (n = 5)	1.7 ± 0.5 x 10^{19}	1.4 ± 0.5 × 10^{19}	.166

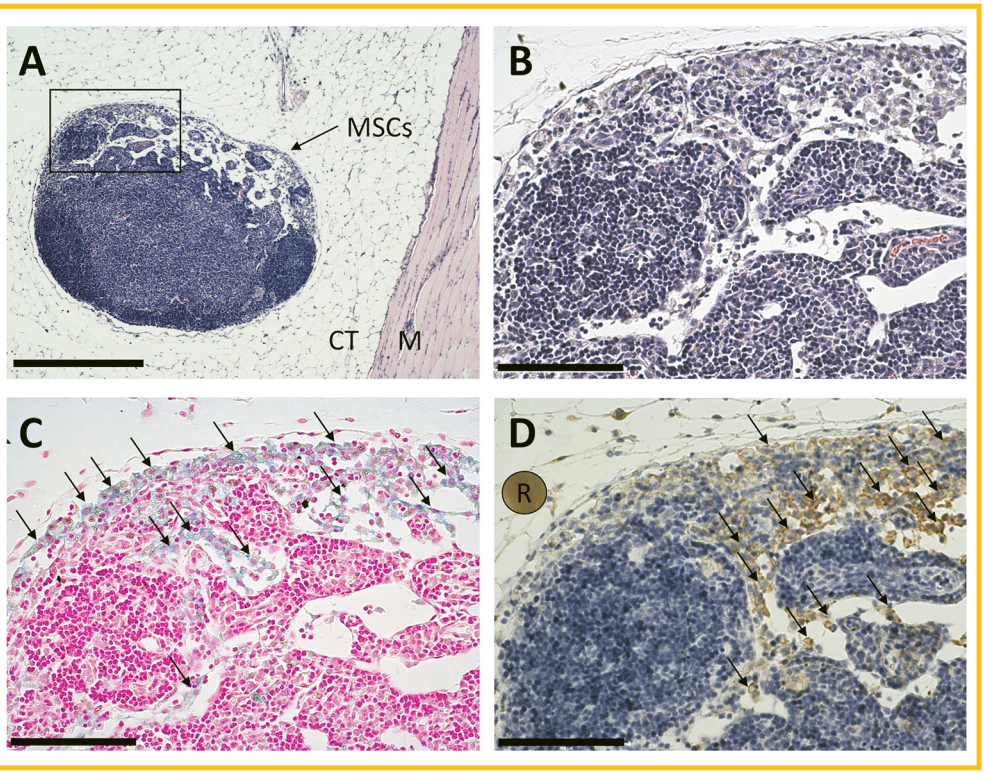

Figure 5. Histological validation showing the presence of MSCs surrounded in connective tissue (CT) and muscle (M) in hematoxylin and eosin (H&E) at 10× magnification (scale bar 500 μm) (A) and 40× magnification (scale bar 100 μm) (B). PPB staining with nuclear fast red counterstain confirms the presence of iron within MSCs (C). Black arrows indicate PPB-positive cells. F4/80 staining with hematoxylin counterstain reveals macrophage infiltration within the same region as the MSCs (D). Expected F4/80 staining is shown in the reference indicator (R). Black arrows indicate F4/80-positive cells. 40× magnification scale bars 100 μm (C, D).

easily compare FWHM and SNR of ferucarbotran (Vivotrax, 5.5 μg iron/μL) in the future. The ideal MPI nanoparticle is still under investigation, considering the effects of nanoparticle size and biological properties, that is, surface composition and cell labeling process. The Langevin model predicts a cubic improvement in spatial resolution with increasing nanoparticle size (23, 25). USPIO (ferumoxytol) nanoparticles have a diameter of $<$50 nm, which is smaller and contain less iron than other available nanoparticles such as SPIOs (50–100 nm) and micron-sized superparamagnetic iron oxides ($\sim$1 μm) (27).

In our study, we used protamine sulfate and heparin to increase uptake of ferumoxytol by MSCs. There is evidence (28) that the use of transfection agents (protamine) can reduce MPI detection; however, this effect is seen mainly at lower drive frequencies (0.4 kHz). The Momentum™ MPI scanner uses a 45 kHz alternating magnetic field to excite iron nanoparticles.

We showed that the formation of a calibration line was a robust technique to quantify iron content from measured MPI signal. In this process, the samples of iron (0.75–30 μg) were imaged using the same settings as the other in vivo scans (3D isotropic mode). This linear relationship persists at low iron concentrations (0.75–3 μg), which is useful in the quantification of ferumoxytol-labeled MSCs (which contained $\sim$2.4 μg in 1×10^6 cells on day 0).

Imaging Inflammation With ^{19}F MRI

This is the first study to use PFC to indicate inflammation associated with iron-labeled stem cells and to track this over time. Following the intravenous administration of PFC, we detected prominent regions of ^{19}F signal in the limb muscle surrounding the MSC implant using ^{19}F MRI. This in vivo labeling technique is known to label resident phagocytic immune cells of the reticuloendothelial system (8, 10). We detected a large number of ^{19}F atoms (on the order of 10^{19}) in the ipsilateral limb on both day 1 and 12. Microscopy obtained on day 12 confirmed that F4/80-positive cells were present in muscle tissue at the site of implantation. This suggests that the number of PFC-positive macrophages remained constant over this time. We can get a rough estimate of macrophage cell number by comparing the value for total ^{19}F atoms with the mean ^{19}F uptake per cell for macrophages labeled in vitro. Our previous work has measured 2.12×10^{11} ^{19}F spins per macrophage using NMR (21). Using this value, we would estimate that $\sim 7.44 \times 10^7$ cells are present at the site of the MSC implantation on day 1 and 6.93×10^7 cells on day 12.

This is the first study to demonstrate the ability to image macrophage infiltration in vivo using ^{19}F on a clinical (3 T) MRI system. Compared with iron-based cell tracking, ^{19}F MRI has lower sensitivity and consequently, preclinical ^{19}F cell tracking has only been performed at relatively high magnetic field strengths (>3 T). The bSSFP imaging sequence and surface RF coil play a major role in enhancing sensitivity to enable detection and cell tracking of ^{19}F-positive cells at 3 T.

Potential Limitations

The MRI and MPI cell labeling agents used in this study (iron and PFC) may be diluted over time as cells proliferate, and thus, there is some ambiguity in the number of cells detected. Since MSCs are implanted in vivo to a suppressive environment that lacks nutrients, we do not expect that MSCs are proliferating substantially. We presume that the reduction ferumoxytol in MSCs, by detection of voids in ^{1}H MRI and by MPI, is predominately

resulting from MSC death. The presence and detection of ferumoxytol do not reflect cell viability because this agent is retained within apoptotic MSCs. Phagocytic immune cells uptake these apoptotic MSCs and the USPIO nanoparticles for clearance in the liver. Thus, immune cells may be labeled with PFC and ferumoxytol, in a process called bystander labeling. Hitchens et al. (29) previously showed that if iron and ^{19}F agents are in the same cell, iron-mediated quenching of ^{19}F signal can occur. This may contribute to ambiguity when detecting and quantifying PFC-labeled macrophages that are involved with clearance of MSCs. However, we did not detect a difference in ^{19}F signal between mice, which received ferumoxytol-labeled MSCs or unlabeled MSCs. This indicates that while quenching of ^{19}F signal may be occurring in the presence of ferumoxytol, this effect does not significantly alter the quantification of PFC-labeled macrophages in this application.

We detected unwanted signal in the mouse gut in all 5 mice imaged with MPI (Figure 3) owing to the presence of iron in mouse feed. This gut signal is also present in mice that do not have iron-labeled cells implanted (data not shown). This signal can complicate analysis of MPI using the automatic thresholding tool if the gut signal is much brighter than the region of interest. Because of this, the signal from ferumoxytol-labeled MSCs was manually delineated for 3 of the mice on day 12. This has negligible impact on the signal quantification, rather it is more time-consuming for the user. This gut signal can also create problems if it is in close proximity to other target sources of iron. This did not impact the quantification of iron in this study, as the gut signal was distant enough from the MSC implant; however, this should be considered when designing future experiments.

The in vivo scan times for MPI (1 h) are considerably longer than MRI (9 minutes for ^{1}H scans and 18 minutes for ^{19}F scans). This much time under anesthesia is undesirable for cell tracking when images are collected at multiple time points. Although 2-dimensional MPI scans of mice can be acquired within 3 minutes, these images (which appear as maximum intensity projections) do not have volumetric data for accurate quantification of iron present within a 3D geometry.

CONCLUSION

In this study, we have shown that iron-based ^{1}H MRI, ^{19}F MRI, and MPI can be used together to noninvasively monitor the fate of 2 cell populations in vivo (MSCs and macrophages). This is the first time that these 3 modalities are combined to monitor cell populations in vivo. We propose that these cellular imaging techniques could be used to monitor MSC engraftment over time and detect the infiltration of macrophages at transplant sites. This could enhance therapeutic monitoring to confirm appropriate MSC delivery, measure the number of MSCs present over time, and quantify immune infiltrate to identify MSC rejection.

Supplemental Materials

Supplemental Figure 1: https://doi.org/10.18383/j.tom.2019.00020.sup.01

Supplemental Figure 2: https://doi.org/10.18383/j.tom.2019.00020.sup.02

ACKNOWLEDGMENTS

We acknowledge the following sources of funding for OCS: Natural Sciences and Engineering Research Council, Molecular Imaging Graduate Program (Western University), Translational Breast Cancer Research Unit, Ontario Graduate Queen Elizabeth II Scholarship, and Cancer Research and Technology Transfer Program.

Conflict of Interest: None reported.

Disclosures: No disclosures to report.

REFERENCES

1. Le Blanc K, Ringdén O. Immunobiology of human mesenchymal stem cells and future use in hematopoietic stem cell transplantation. Biol Blood Marrow Transplant. 2005;11:321–334.
2. Samsonraj RM, Raghunath M, Nurcombe V, Hui JH, van Wijnen AJ, Cool SM. Concise review: multifaceted characterization of human mesenchymal stem cells for use in regenerative medicine. Stem Cells Transl Med. 2017;2:2173–2185.
3. Gao F, Chiu SM, Motan DAL, Zhang Z, Chen L, Ji HL, Tse HF, Fu QL, Lian Q. Mesenchymal stem cells and immunomodulation: current status and future prospects. Cell Death Dis. 2016;7 :e2062.
4. Li N, Hua J. Interactions between mesenchymal stem cells and the immune system. Cell Mol Life Sci. 2017;74:2345–2360.
5. Meirelles LDS, Nardi NB. Methodology, biology and clinical applications of mesenchymal stem cells. Front Biosci (Landmark Ed). 2009;14:4281–4298.
6. Borgovan T, Crawford L, Nwizu C, Quesenberry P. Stem cells and extracellular vesicles: biological regulators of physiology and disease. Am J Physiol Cell Physiol. 2019;317:C155–C166.
7. Salazar-Noratto GE, Luo G, Denoeud C, Padrona M, Moya A, Bensidhoum M, Biozios R, Potier E, Logeart-Avramoglou D, Petite H. Concise review: Understanding and leveraging cell metabolism to enhance mesenchymal stem cell transplantation survival in tissue engineering and regenerative medicine applications. 2019. Stem Cells [Epub ahead of print]
8. Gaudet JM, Hamilton AM, Chen Y, Fox MS, Foster PJ. Application of dual 19F and iron cellular MRI agents to track the infiltration of immune cells to the site of a rejected stem cell transplant. Magn Reson Med. 2017;78:713–720.
9. Makela AV, Murrell DH, Parkins KM, Kara J, Gaudet JM, Foster PJ. Cellular imaging with MRI. Top Magn Reson Imaging. 2016;25:177–186.
10. Khurana A, Nejadnik H, Gawande R, Lin G, Lee S, Messing S, Castaneda R, Derugin N, Pisani L, Lue TF, Daldrup-Link HE. Intravenous ferumoxytol allows noninvasive MR imaging monitoring of macrophage migration into stem cell transplants. Radiology. 2012;264:803–811.
11. Heyn C, Bowen CV, Rutt BK, Foster PJ. Detection threshold of single SPIO-labeled cells with FIESTA. Magn Reson Med. 2005;53:312–320.
12. Bulte J. Superparamagnetic iron oxides as MPI tracers: a primer and review of early applications. Adv Drug Deliv Rev. 2019;138:293–301.
13. Nejadnik H, Pandit P, Lenkov O, Lahiji AP, Yerneni K, Daldrup-Link HE. Ferumoxytol can be used for quantitative magnetic particle imaging of transplanted stem cells. Mol Imaging Biol. 2019;21:465–472.
14. Aghighi M, Theruvath AJ, Pareek A, Pisani LL, Alford R, Muehe AM, Sethi TK, Holdsworth SJ, Hazard FK, Gratzinger D, Luna-Fineman S, Advani R, Spunt SL, Daldrup-Link HE. Magnetic resonance imaging of tumor-associated macrophages: clinical translation. Clin Cancer Res. 2018;24:4110–4118.
15. Gaudet JM, Ribot EJ, Chen Y, Gilbert KM, Foster PJ. Tracking the fate of stem cell implants with fluorine-19 MRI. PLoS One. 2015;10:1–12.
16. Chapelin F, Capitini CM, Ahrens ET. Fluorine-19 MRI for detection and quantification of immune cell therapy for cancer. J Immunother Cancer. 2018;6:1–11.
17. Bulte JWM, Walczak P, Janowski M, Krishnan KM, Arami H, Halkola A, Gleich B, Rahmer J. Quantitative "hot-spot" imaging of transplanted stem cells using superparamagnetic tracers and magnetic particle imaging. Tomography. 2015;1:91–97.
18. Dousset V, Delalande C, Ballarino L, Quesson B, Seilhan D, Coussemacq M, Thiaudiére E, Brochet B, Canioni P, Caillé J-M. In vivo macrophage activity imaging in

the central nervous system detected by magnetic resonance. Magn Reson Med. 1999;41:329–333.
19. Thu MS, Henry Bryant L, Coppola T, Kay Jordan E, Budde MD, Lewis BK, Chaudhry A, Ren J, Varma NK, Arbab AS, Frank JA. Self-assembling nanocomplexes by combining ferumoxytol, heparin and protamine for cell tracking by MRI. Nat Med. 2012;18:463–467.
20. Mcfadden C, Mallett CL, Foster PJ. Labeling of multiple cell lines using a new iron oxide agent for cell tracking by MRI. Contrast Media Mol Imaging. 2011;6:514–522.
21. Makela AV, Foster PJ. Preclinical 19 F MRI cell tracking at 3 Tesla. MAGMA. 2019;32:123–132.
22. Goodwill PW, Conolly SM. The X-space formulation of the magnetic particle imaging process: 1-D signal, resolution, bandwidth, SNR, SAR, and magnetostimulation. IEEE Trans Med Imaging. 2010;29:1851–1859.
23. Tay ZW, Hensley DW, Vreeland EC, Zheng B, Conolly SM. The relaxation wall: experimental limits to improving MPI spatial resolution by increasing nanoparticle core size. Biomed Phys End Express. 2017;3:1–21.
24. Houston WV. A compound interferometer for fine structure work. Phys Rev. 1927
25. Arami H, Ferguson RM, Khandhar AP, Krishnan KM. Size-dependent ferrohydrodynamic relaxometry of magnetic particle imaging tracers in different environments. Med Phys. 2013;40:1–14.
26. Noad J, Gonzalez-Lara LE, Broughton HC, McFadden C, Chen Y, Hess DA, Foster PJ. MRI tracking of transplanted iron-labeled mesenchymal stromal cells in an immune-compromised mouse model of critical limb ischemia. NMR Biomed. 2013;26:458–467.
27. Modo M, Hoehn M, Bulte J. Cellular MR imaging. Mol Imaging. 2005;4:143–164.
28. Suzuka H, Mimura A, Inaoka Y, Murase K. Magnetic Nanoparticles in Macrophages and Cancer Cells Exhibit Different Signal Behavior on Magnetic Particle Imaging. J Nanosci Nanotechnol. 2019;19:6857–6865.
29. Hitchens TK, Liu L, Foley LM, Simplaceanu V, Ahrens ET, Ho C. Combining perfluorocarbon and superparamagnetic iron-oxide cell labeling for improved and expanded applications of cellular MRI. Magn Reson Med. 2015;73:367–375.